Journal of Engineering Physics and Thermophysics, Vol. 81, No. 2, 2008

SIMULATION OF A SUBSONIC ISOTHERMAL TURBULENT SUBMERGED JET FLOWING FROM AN ANNULAR NOZZLE

K. N. Volkov

UDC 532.529

A simulation of the flow in a jet has been carried out with the use of the Reynolds-averaged, space-filtered Navier–Stokes equations closed by the k–ε model of turbulence and the subgrid RNG model of eddy viscosity. The results of calculations carried out on the basis of the k–ε model and the results of simulation of large vortices are in quantitative and qualitative agreement with the corresponding measurement data, which is evidence in favor of the main laws defining the decay of the gas-dynamic behavior of cold-gas submerged jets and the fluctuations of their parameters.

Introduction. In the literature, for example in [1, 2], there is a vast amount of material on mathematical simulation of subsonic isothermal turbulent submerged jets and jets in cocurrent flows and on measurement of their characteristics.

The characteristics of incompressible-fluid and compressible-gas jets were measured in [3] (the kinetic-energy balance and the averaged and fluctuating parameters at $\mathrm{Re} = 10^5$), [4] (the fluctuations of the longitudinal velocity at $0.02 \le M \le 0.96$ and $10^4 \le \mathrm{Re} \le 5.9\cdot10^5$), [5] (the distributions of the kinetic turbulent energy and the rate of its dissipation in the initial region of a jet, the Taylor microscale and integral scale of turbulence), [6] (the rate of dissipation of the kinetic turbulent energy), [7] (the turbulent diffusion and the correlations of the velocity and concentration at $\mathrm{Re} = 1.1\cdot10^4$), [8] (the moments of velocity measured to the third order at $\mathrm{Re} = 9.55\cdot10^4$, [9] (the jet in a cocurrent flow and the correlation moments of velocity and concentration fluctuations measured to the third order at $\mathrm{Re} = 1.05\cdot10^4$).

The approximate approaches used for description of the flow in a jet are based on the semiempirical Prandtl and Taylor theories of free turbulence and involve consideration of the initial and main regions of a flow on the assumption that the distributions of the excess momentum at the cross sections of the jet are locally similar [1, 2].

Numerical calculations were carried out with different models of turbulence, in particular the model of mixing [1], the k–ε model [10, 11], and the equations of transfer of Reynolds stresses [12].

The similarity of the flows in a jet and in the boundary layer allows one to write the Reynolds-averaged Navier–Stokes equations in the parabolic form and numerically integrate them effectively. For simplicity, the coordinates used are transformed on condition that the excess-momentum flow in an isobaric jet is constant, which makes it possible to use a computational region in the form of a finite-size band instead of the infinitely large region of integration in physical variables [11, 12]. New independent variables can be used in the case where the excess-velocity profile is monotone; this condition is usually fulfilled at any distance from the exit section of a nozzle. Since boundary layers are formed at the inner and outer walls of the nozzle, the distribution of the parameters of the flow at the initial cross section is nonmonotone, which changes the excess momentum of the jet.

Numerical integration of the Reynolds-averaged Navier–Stokes equations allows one to obtain the distributions of the time-average and fluctuating characteristics of a flow. The calculation data on the velocity distribution, obtained with the use of the k–ε model, are in good agreement with the corresponding measurement data; however, the calculations of the kinetic turbulent energy and the degree of expansion of a jet give overstated values of these quantities. If there is a cocurrent flow, the calculated values of the velocity exceed the measured ones [1, 10, 11].

One of the features of the free shear flows is the presence of large-scale vortex formations in the mixing layer [13]. Control of coherent structures by amplification or destruction of them, for example with the use of acoustic

University of Surrey, Guildford, GU2 7XH, Great Britain; email: dsci@mail.ru. Translated from Inzhenerno-Fizicheskii Zhurnal, Vol. 81, No. 2, pp. 312–320, March–April, 2008. Original article submitted November 9, 2006.

waves of different intensity and frequency, makes it possible to effectively act on the processes of transfer and heat exchange.

The topology of large-scale vortex structures in the mixing layer is investigated experimentally and by numerical simulation [13]. In the calculations, methods of direct numerical simulation, methods of simulations of large vortices, and combined methods are used.

A direct numerical simulation and a simulation of large vortices of the flow in an incompressible-fluid jet were carried out in [14] ($\mathrm{Re} = 3.6\cdot10^3$, [15] ($\mathrm{Re} = 10^4$, [16] ($\mathrm{Re} = 2\cdot10^3$ and $\mathrm{Re} = 10^4$), [17] ($\mathrm{Re} = 4\cdot10^3$), and [18] ($\mathrm{Re} = 2.5\cdot10^4$). As a subgrid model, the Smagorinskii model [15, 18], the structural-function model [17] (it is reduced to the Smagorinskii model under certain conditions), and the model of similar scales [15] are used. Some calculations are carried out in the axisymmetric formulation [15]. A comparison of the calculation data with the measurement data has shown that the Smargonskii model understimates the intensity of the turbulence in the mixing zone [15]. The disagreement between the data is explained by the intermittancy of the flow and the reverse transfer of energy from the small vortices to the large ones (unlike the model of similar scales, the Smagorinskii model takes no account of the reverse energy transfer). The authors of [16], take the notion of direct numerical simulation to mean approaches in which the eddy viscosity is determined by the pitch of a difference grid. The calculations carried out in [16] allow one to simulate a turn of axes in a free rectangular jet and define the anisotropic spreading along a wall in the direction perpendicular to the axis of the jet flowing from an annular nozzle. The mixing of different-density jets was considered in [17]. In [18], prominence was given to the processes of formation of a mixing layer in the initial region of a jet, the development of this layer downstream of the flow, and the influence of the coefficient of the subgrid Smagorinskii model on the characteristics of the jet.

Incompressible-gas jets were investigated in [19] ($\mathrm{M} = 0.9$, $\mathrm{Re} = 3.6\cdot10^4$, [20] ($\mathrm{Re} = 6\cdot10^3$ and $\mathrm{Re} = 10^5$), [21] ($\mathrm{Re} = 7.6\cdot10^3$ and $\mathrm{Re} = 2.76\cdot10^4$), [22] ($\mathrm{M} = 0.9$, $\mathrm{Re} = 10^4$), [23] ($\mathrm{M} = 0.9$, $\mathrm{Re} = 10^4$), [24] ($\mathrm{M} = 0.9$, $2.5\cdot10^3 \le \mathrm{Re} \le 4\cdot10^5$). As a subgrid model, the Smagorinskii model [21] and the dynamic model of [19–21] were used. In [22, 23], the calculations were carried out on a coarse grid without recourse to any subgrid model, and the dissipation mechanism was introduced by the difference scheme (this approach is given the name monotonically integrated LES). The data obtained in [24] point to the fact that the approach based on the explicit filtration of the Navier–Stokes equations and the approximate decomposition of the velocity field is promising. The data of numerical simulation are used for determining the sound field of a jet [19, 22, 23] as well as for investigating the methods of external action on the structure of a jet and intensification of the turbulent mixing [20].

The calculations of incompressible-fluid jets [14–18] and compressible-gas jets [19–24] were carried out for a fairly narrow range of parameters characterizing the outflow of a jet with the use of a coarse grid. In a number of works, for example in [15], the axisymmetric formulation of the problem, representing a three-dimensional approach, was used, which is in contradiction with the views on simulation of large vortices. A comparatively small number of works are devoted to the study of the characteristics of the near flow in a jet.

In the present work, the flow in a jet was defined using the approach based on the solution of the Reynolds-averaged Navier–Stokes equations, and large vortices were simulated by integration of the space-filtered Navier–Stokes equations. The main equations were closed with the use of the k–ε model of turbulence and the subgrid RNG model of eddy viscosity. The results of calculations were compared to one another by the average parameters of the flow and to the data of a physical experiment.

Main Equations. We consider a subsonic turbulent submerged jet flowing from an annular nozzle. The origin of coordinates is positioned at the nozzle exit section. The direction of the positive x coordinate is coincident with the direction of propagation of the jet. As the characteristic scales, the radius of the nozzle exit section r_a was used for the variables with the dimensions of length, and the velocity u_a and temperature T_a of the gas at the nozzle exit section were used for the variables with the dimensions of velocity and temperature. It is assumed that the gas temperature at the nozzle exit section is equal to the temperature of the environment.

Equations in conservative variables. In the Cartesian coordinate system (x, y, z), a nonstationary flow of a viscous compressible gas is described by the following equation:

$$\frac{\partial \mathbf{Q}}{\partial t} + \frac{\partial \mathbf{F}_x}{\partial x} + \frac{\partial \mathbf{F}_y}{\partial y} + \frac{\partial \mathbf{F}_z}{\partial z} = \mathbf{H}, \qquad (1)$$

which is supplemented by the equation of state of a perfect gas

$$p = (\gamma - 1)\,\rho\left[e - \frac{1}{2}\left(v_x^2 + v_y^2 + v_z^2\right)\right].$$

The vector of conservative variables $\mathbf{Q}$ and the vectors of flows $\mathbf{F}_x$, $\mathbf{F}_y$, $\mathbf{F}_z$ have the following form:

$$\mathbf{Q} = \begin{pmatrix} \rho \\ \rho v_x \\ \rho v_y \\ \rho v_z \\ \rho e \end{pmatrix}, \quad \mathbf{F}_x = \begin{pmatrix} \rho v_x \\ \rho v_x v_x + p - \tau_{xx} \\ \rho v_x v_y - \tau_{xy} \\ \rho v_x v_z - \tau_{xz} \\ (\rho e + p)\, v_x - v_x\tau_{xx} - v_y\tau_{xy} - v_z\tau_{xz} + q_x \end{pmatrix},$$

$$\mathbf{F}_y = \begin{pmatrix} \rho v_y \\ \rho v_y v_x - \tau_{yx} \\ \rho v_y v_y + p - \tau_{yy} \\ \rho v_y v_z - \tau_{yz} \\ (\rho e + p)\, v_y - v_x\tau_{yx} - v_y\tau_{yy} - v_z\tau_{yz} + q_y \end{pmatrix}, \quad \mathbf{F}_z = \begin{pmatrix} \rho v_z \\ \rho v_z v_x - \tau_{zx} \\ \rho v_z v_y - \tau_{zy} \\ \rho v_z v_z + p - \tau_{zz} \\ (\rho e + p)\, v_z - v_x\tau_{zx} - v_y\tau_{zy} - v_z\tau_{zz} + q_z \end{pmatrix}.$$

The components of the viscous-stress tensor and the components of the heat-flow vector are determined from the relations

$$\tau_{ij} = \mu_e\left(\frac{\partial v_i}{\partial x_j} + \frac{\partial v_j}{\partial x_i} - \frac{2}{3}\frac{\partial v_k}{\partial x_k}\delta_{ij}\right), \quad q_i = -\lambda_e\frac{\partial T}{\partial x_i}.$$

Equation (1) can be used for the description of both laminar and turbulent flows. In simulation of turbulent flows, the effective viscosity is calculated as the sum of the molecular and eddy viscosities, and the effective heat conduction is expressed in terms of the eddy viscosity and the Prandtl number.

The boundary conditions are set and the calculation data are processed in the cylindrical (x, r, θ) and not the Cartesian coordinate system (x, y, z). The radial and circular velocity components are related to the Cartesian velocity components by the relations

$$v_r = \frac{v_y y + v_z z}{(y^2 + z^2)^{1/2}}, \quad v_\theta = \frac{v_z y + v_y z}{(y^2 + z^2)^{1/2}}.$$

Because of the symmetry of the computational region and the boundary conditions, the time-average circular velocity is equal to zero.

Equations of the model of turbulence. Equation (1) is written in time-average quantities. The statistical characteristics of turbulence are determined by the two-parameter k–ε model of turbulence with Launder corrections for constants c_μ and $c_{\varepsilon 2}$ [25].

The equations of the k–ε model of turbulence have the following form:

$$\frac{\partial \rho k}{\partial t} + (\rho\mathbf{v}\cdot\nabla)\,k = \nabla\left[\left(\mu + \frac{\mu_t}{\sigma_k}\right)\nabla k\right] + P - \rho\varepsilon\,; \tag{2}$$

$$\frac{\partial \rho\varepsilon}{\partial t} + (\rho\mathbf{v}\cdot\nabla)\,\varepsilon = \nabla\left[\left(\mu + \frac{\mu_t}{\sigma_\varepsilon}\right)\nabla\varepsilon\right] + \frac{\varepsilon}{k}\,(c_{\varepsilon 1}P - c_{\varepsilon 2}\rho\varepsilon)\,. \tag{3}$$

The term defining the production of turbulence is determined from the relation

$$P = \mu_t \left| S \right|^{1/2} \left| \Omega \right|^{1/2},$$

where

$$\left| S \right| = (2S_{ij}S_{ij})^2; \quad \left| \Omega \right| = (2\Omega_{ij}\Omega_{ij})^2; \quad S_{ij} = \frac{1}{2}\left(\frac{\partial v_i}{\partial x_j} + \frac{\partial v_j}{\partial x_i}\right); \quad \Omega_{ij} = \frac{1}{2}\left(\frac{\partial v_i}{\partial x_j} - \frac{\partial v_j}{\partial x_i}\right).$$

The turbulent viscosity is calculated by the Kolmogorov–Prandtl formula $\mu_t = c_\mu \rho k^2/\varepsilon$. We assign to the constants of the model of turbulence the following values: $c_\mu = 0.09$, $\sigma_k = 1.0$, $\sigma_\varepsilon = 1.3$, $c_{\varepsilon 1} = 1.44$, $c_{\varepsilon 2} = 1.92$, and $\mathrm{Pr_t} = 0.7$. The Launder corrections to these constants are determined as [25]

$$c_\mu = 0.09 - 0.04f, \quad c_{\varepsilon 2} = 1.92 - 0.0667f,$$

where

$$f = \left| \frac{\delta}{2\Delta u}\left(\frac{du_c}{dx} - \left|\frac{du_c}{dx}\right|\right)\right|.$$

The term Δu means the characteristic difference between the velocities. The thickness of the mixing zone is determined on condition that the excess-momentum pulse is equal to zero.

Subgrid model. Equation (1) is written relative to the space-filtered quantities. In the subgrid model of viscosity constructed on the basis of the theory of renormalized groups, the calculation of the effective viscosity is reduced to the solution of the nonlinear algebraic equation [26]

$$\mu_e = \mu\,[1 + H(X - A)]^{1/3}, \quad X = \frac{\mu_s^2 \mu_e}{\mu^3},$$

where $A = 100$. The subgrid viscosity is determined from a relation that differs from the Smagorinskii model by a constant factor:

$$\mu_s = \rho\,(C_R \Delta)\,\left| S \right|^2,$$

where $C_R = 0.157$. At $X >> C$, the Smagorinskii formula with a model coefficient $C_S = (2C_R)^{1/4}/(2\pi) = 0.119$ is obtained.

In the completely turbulent region of flow, $\mu_s >> \mu$; therefore, $\mu_e \approx \mu_s$ and the RNG model is reduced to the Smagorinskii model. In the weakly turbulent region, the argument of the Heaviside function became negative, which is why $\mu_e \approx \mu$. A correct representation of the effective viscosity in the laminar and completely turbulent regions of the flow makes it possible to use the RNG model for calculating the transient regimes of flow.

In the case of fairly low values of the turbulent Mach number (at $\mathrm{M_t} < 0.4$), the correction for the compressibility weakly influences the results of calculations [27].

The width of the filter Δ is related to the size of the pitch of a difference grid:

$$\Delta = V^{1/3} = (\Delta x \Delta y \Delta z)^{1/3},$$

where Δx, Δy, Δz are the grid pitches in the coordinate directions x, y, z.

Initial and Boundary Conditions. The conditions of outflow of the jet being considered weakly influence the characteristics of the flow at fairly high Reynolds numbers ($\mathrm{Re} > 5 \cdot 10^4$), moderate Mach numbers, and an initial level of turbulence that does not exceed 3–4% [4].

The input boundary of the computational region is coincident with the nozzle exit section ($x = 0$), and, for the velocity at it, the following boundary conditions are set:

$$v_x(r) = \begin{cases} u_a(r), & |r| \le r_a; \\ 0, & |r| > r_a. \end{cases}$$

At the portion of the boundary, coincident with the nozzle exit section (at $|r| \le r_a$), the distributions of the velocity, temperature, and turbulence characteristics are fixed. In the core of the flow (at $|r| \le 0.9r_a$) these parameters are held constant ($v_x = u_a$, $T = T_a$, $k = k_a$, $\varepsilon = \varepsilon_a$), and near the walls of the nozzle at $0.9 \le r_a|r| \le r_a$ the velocity and turbulent viscosity decrease, as the wall is approached, to zero values by the power law. The derivative of the static pressure with respect to the normal to the boundary is taken to be equal to zero.

When large vortices, caused by the pulsations of the flow in a jet, are simulated, nonstationary boundary conditions should be set at the input cross section [16]. The free shear flows are unstable, and oscillations in them arise in the absence of external sources of disturbances.

To formulate the boundary conditions correctly, it is necessary to calculate the flows in the circular tube and the boundary layer at the outer surface of the nozzle [21, 23] (a part of the nozzle falls within the computational region). Since this problem is laborious, the flow in the tube is not calculated and, at the nozzle exit section, the velocity profile, on which accidental sinusoidal disturbances are emposed, is determined [19]:

$$v_x(r, t) = \frac{u_a}{3}\left[1 + \tanh\left(\frac{0.5 - |r|}{2\delta}\right)\right]\left[1 + \alpha \sin\ (\mathrm{St}\, t)\right].$$

In the calculations, $\delta/r_a = 0.1$, $\mathrm{St} = 0.45$, and $\alpha = 0.0025$. Small accidental disturbances are also imposed on the radial distribution of the circular velocity:

$$v_\theta(r, t) = 0.025 \exp\left[-3\,(1 - |r|)^2\right]\varphi,$$

where φ is a random number from the uniform distribution over the interval [–0.5, 0.5]. The radial velocity at the nozzle exit section $v_r(r, t) = 0$.

The boundary conditions away from the submerged jet (at the lower and upper boundaries) following from the nozzle are determined by the ejection properties of the jet — away from the jet there exists an induced potential flow directed to the jet. The properties and parameters of this flow are unknown in advance and are determined by the jet itself. An incorrect formulation of the velocity distribution at the outer boundary of the computational region distorts the field of the flow [16]. The calculations of stationary flows show that the best results are obtained with the boundary conditions determined on the basis of an exact solution defining the potential flow outside the turbulent circular jet [28].

In the process of solving the Reynolds equations the static pressure is determined at the output of the computational region and the velocity components are extrapolated with an accuracy to the first order from within the computational region (soft boundary conditions). When the method of large vortices is realized at the boundaries, through which gas comes out from the computational region, nonreflecting boundary conditions (convective-transfer conditions) are used for the velocity. It is assumed that the gas is at rest at the initial instant of time ($v_x = v_y = v_z = 0$, $p = 1.013 \cdot 10^5$ Pa, $T = 288$ K).

Numerical Method. The discretization of Eq. (1) and the equations of the model of turbulence (2) and (3) is carried out by the control-volume method and the difference schemes of high time and space resolution [29]. The time discretization is carried out with the use of the five-step Runge–Kutta method, and the convective and viscous flows are discretized using the modified MUSCL scheme and centered difference formulas of the second order.

The system of difference equations is solved by the multigrid method on the basis of the complete-approximation scheme. As the smoothing algorithm, the generalized method of weighted discrepancies is used. A sequence of embedded grids is constructed using the method of collapsible faces [29]. To prevent instability of the numerical solution in the low-velocity regions of the flow, the Jacobi method of block preconditioning is used in the calculations based on the compressible Navier–Stokes equations. The computational procedure is realized in the form of a machine code in the Fortran programming language and the C/C++ language. The computational procedure is parallelized with

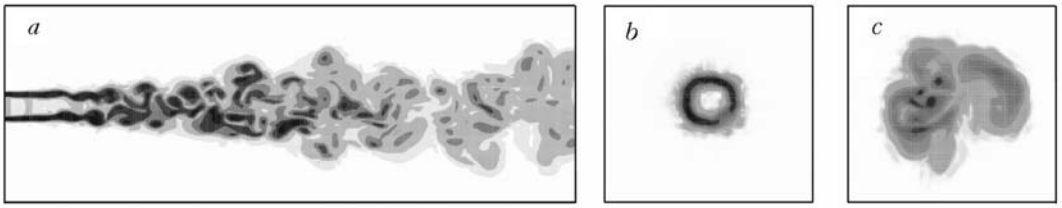

Fig. 1. Lines of the velocity-vortex level at the instant $t = 0.15$ sec at the middle cross section of the jet (a) and at the sections $x/r_a = 10$ (b) and $x/r_a = 80$ (c).

the use of the MPI interface of interprocessor interaction. The calculations where carried out on an IBM SP/1600 supercomputer with eServer–pServer-690 units and a Power 4+ processor operating at 1.7 GHz. The supercomputer center is located at the Central laboratory (Daresbury Laboratory) of the Research Councils in Warrington (United Kingdom).

Results of Calculations. The initial parameters were as follows: $r_a = 5$ mm, $u_a = 50$–210 m/sec, $T_a = 300$ K, $p_a = 1.013 \cdot 10^5$ Pa, $k_a = 0.01u_a^2$, $\varepsilon_a = 0.002u_a^2/r_a$. The parameters of the flow at the cut of the nozzle correspond to the Mach numbers $0.14 \le M \le 0.68$ and the Reynolds numbers $3.45 \cdot 10^4 \le Re \le 1.72 \cdot 10^5$.

The computational region had the form of a truncated pyramid. The length of the computational region was equal to $L_x = 250r_a$. It was assumed that its width and height are equal to $L_y = L_z = 10r_a$ at the input cross-section and $L_y = L_z = 40r_a$ at the output cross section.

At $Re = 1.72 \cdot 10^5$ (the largest Reynolds number used in the calculations), a grid containing $350 \times 150 \times 150 = 7{,}875{,}000$ nodes was used. The grid was bunched in the longitudinal direction to the cut of the nozzle. It was assumed that the pitch downstream of the cross section $x = 15r_a$ is practically constant with respect to the variable x and then increases gradually by the geometric progression law. The grid at the cross section of the nozzle is bunched to the edges of the nozzle. The pitches along the coordinate directions are as follows: $\Delta x_{min} = 0.08r_a$, $\Delta x_{max} = 0.25r_a$, $\Delta y_{min} = \Delta z_{min} = 0.02r_a$, $\Delta y_{max} = \Delta z_{max} = 0.1r_a$. The time step $\Delta t = 0.1r_a/u_a$. The calculations were carried out until $\Delta t = 2000r_a/u_a$.

The Kolmogorov and Taylor microscales of length in a circular jet are related to the Reynolds number at the cut of the nozzle and the axis coordinate (at $x/r_a > 140$) by the relations [6, 9]

$$l_K = (48\mathrm{Re}^3)^{-1/4} x, \quad l_T = 0.88\mathrm{Re}^{-1/2} x.$$

In the range of Reynolds numbers being considered, we obtain that $4.5 \cdot 10^{-5} \le l_K/x \le 1.5 \cdot 10^{-5}$ and $2.12 \cdot 10^{-3} \le l_T/x \le 4.73 \cdot 10^{-3}$. At $Re = 1.72 \cdot 10^5$ and $x/r_a = 150$, $\Delta x_{max} = 8l_K$ and $\Delta y_{max} = \Delta z_{max} = 6l_K$.

An instantaneous pattern of flow in the jet is visualized with the use of the velocity vortex defined as

$$\Omega = |\nabla \times \mathbf{v}| = \left(\Omega_x^2 + \Omega_y^2 + \Omega_z^2\right)^{1/2}.$$

The lines of the velocity-vortex level at the cross sections of the jet flow are presented in Fig. 1.

In the shear layer of the jet there are large-scale vortex structures having the form of toroidal axially symmetric vortices arising at any distance from the nozzle exit section (this distance is equal to 1–2 diameters of the nozzle) and propagating in the mixing layer downstream of the flow. The coherent structures at the radial cross section of the jet represent ellipses, which is evidence of the anisotropy of the turbulent pulsations in the region where there are large-scale vortices. The vortex structures in the initial region of the jet have a fairly small characteristic scale. Downstream of the initial region, vortices of larger characteristic scale arise; in this case, the momentum exchange between the jet and the surrounding fluid intensifies.

The generation of vortices is due to the Kelvin–Helmholtz instability of the shear layer. The maximum and minima of the vorticity are approximately at the center of the vortices. At small Reynolds numbers, the jet near the nozzle exit section is practically axisymmetric. When the Reynolds number increases to $Re = 10^4$, with increase in the

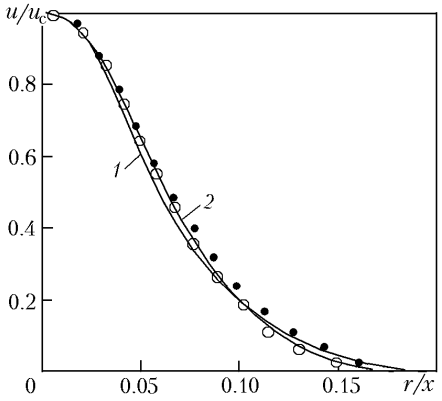

Fig. 2. Profiles of the longitudinal velocity compared to the data of [3] (dark points) and [7] (light points): 1) calculation by the k–ε model; 2) results of simulation of large vortices.

distance from the nozzle exit section there appears a weak sinusoidal wave. A further increase in the Reynolds number results in the flow becoming completely three-dimensional and turbulent.

The profiles of the average longitudinal velocity normalized to the velocity at the axis of the jet are practically universal at $x/r_a > 80$ (Fig. 2, Re = 10^5), which agrees with the measurement data [3, 7]. The results of calculations by the k–ε model and the method of simulation of large vortices are in fairly good agreement. In this case, the first model gives a less filled velocity profile at the cross section of the jet.

The development of the secondary flows in the jet is determined by the correlations $\langle v_r'^2 \rangle$, $\langle v_\theta'^2 \rangle$, and $\langle v_r' v_\theta' \rangle$; in this case, $\langle v_r' v_\theta' \rangle = 0$ in the circular axisymmetric jet.

The root-mean-square value of the longitudinal-velocity pulsations at the axis of the jet (at $x/r_a > 80$) exceeds the corresponding value of the radial velocity by approximately 10–12%, which agrees with the data of [3]; according to these data, the indicated difference is 12–16%. A similarity between the profiles of the longitudinal-velocity fluctuations was detected at $x/r_a > 140$ (Fig. 3a), and a similarity between the fluctuations of the radial and circular velocities was detected at $x/r_a > 180$ and $x/r_a > 200$ respectively (Fig. 3b and c). The calculation results presented correspond to Re = 10^5. The intensities of turbulence in the radial, circular, and axial directions are of the same order of magnitude (approximately 0.22, 0.24, and 0.27 for the radial, circular, and longitudinal velocity respectively). Note that the distribution of longitudinal-velocity fluctuations has a local maximum, while such a maximum is absent in the distributions of the radial-velocity and circular-velocity fluctuations. The largest difference between the results obtained and the measurement data was detected in the near-axis region of the jet.

The distributions of the Reynolds stresses are in good agreement with the data of [7, 8], however the quantitative difference at any points reaches 30% (Fig. 4, Re = 10^4). In this case, the data of the physical experiment [3] give a less-filled profile of the Reynolds stresses, and their maximum value is smaller than the calculated one, obtained by simulation of large vortices. In this case, the k–ε model gives a much smaller Reynolds-stress maximum by approximately 1.5 times positioned at larger values of the transformed coordinate r/x as compared to this maximum given by the method of simulation of large vortices and the physical-experiment data. The radial maximum of the Reynolds stresses is positioned at a fairly close distance to the maximum of the average shear stresses detected at $r/x = 0.055$.

The main contribution to the kinetic turbulent energy is made by the turbulence arising due to the velocity gradient as well as by the terms defining the correlation moments of the pressure and velocity-gradient fluctuations. The positions of their maxima correspond to each other and take place at $r/x = 0.05$. The processing of the data obtained in the process of simulation of large vortices and the results of calculations by the k–ε model has shown that the data on the kinetic turbulent energy are in better agreement than the data on the Reynolds-stress distributions.

In the central region of the jet, the triple correlations $\langle v_x' v_r' v_r' \rangle$ and $\langle v_x' v_\theta' v_\theta' \rangle$ have small negative values, which correlates with the data of [7, 8] but is in contradiction with the data of [3]. These quantities have a maximum at $r/x = 0.075$ and change the sign at $r/x = 0.035$.

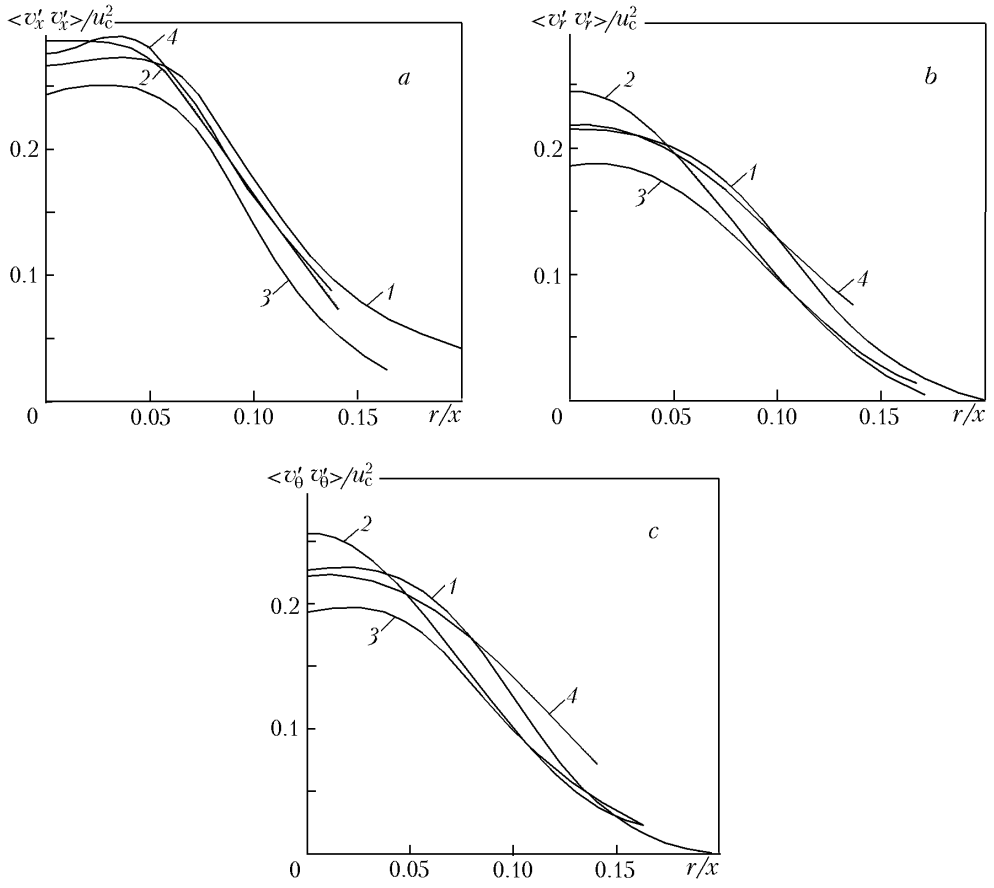

Fig. 3. Distributions of the root-mean-square value of fluctuations of the axial (a), radial (b), and circular (c) velocities determined in the present work (curve 1) and the corresponding data of [3] (curve 2), [7] (curve 3), and [8] (curve 4).

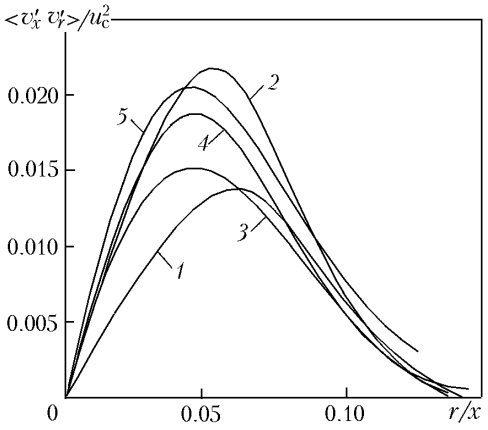

Fig. 4. Distributions of the Reynolds stresses: 1) calculation by the k–ε model; 2) results of simulation of large vortices; 3) data of [3]; 4) data of [7]; 5) data of [8].

The distributions of the velocity fluctuations over the cross sections of the initial and main regions of the jet are locally similar only in the outer zone of mixing (at $r/\delta > 0.3$). The large spread of the experimental data near the boundary of the jet is explained by the fact that the flow is intermittent in character. The maximum value of the turbulent pulsations in the mixing zone reaches 15–16% of the average velocity at a degree of turbulence at the nozzle-

exit section of 1.5–2% (jets with a natural initial turbulence). Downstream of the flow, the fluctuations of the longitudinal velocity at the cross section equalize.

An increase in the turbulence at the nozzle exit section intensifies the mixing of a jet with the surrounding gas and decreases the remote action of the jet. In this case, the distributions of the kinetic turbulent energy along the axis of the jet at small and large initial levels of turbulence are substantially different. In the case where the turbulence at the nozzle-exit section is small, the kinetic energy of turbulence initially increases, reaches a maximum, and then decreases slowly. At a high level of turbulence at the nozzle-exit section, the kinetic turbulent energy initially decreases sharply along the axis of the jet, then increases, reaches a maximum, and then decreases downstream by the power law. In the case where the initial turbulence is very large, the kinetic turbulence energy continuously decreases downstream of the flow.

Conclusions. Large vortices in the flow of a subsonic isothermal turbulent submerged jet flowing from a circular nozzle have been simulated. The results of calculations were compared with the results of the numerical simulation carried out on the basis of solution of the Reynolds-averaged Navier–Stokes equations and the equations of the two-parameter k–ε model of turbulence as well as with the data of a physical experiment.

The calculation data are in qualitative and quantitative agreement with the measurement data, which substantiates the main laws on decay of the gas-dynamic behavior of cold-gas submerged jets and the fluctuations of their parameters.

NOTATION

A, constant of the subgrid model; c_μ, $c_{\varepsilon 1}$, $c_{\varepsilon 2}$, constants of the model of turbulence; C_R, C_S, constants of the subgrid model; e, total energy of a unit mass, J/kg; f, damping function; **F**, vector of a flow; **H**, source term; H, Heaviside function; k, kinetic turbulent energy, m^2/sec^2; l_K, Kolmogorov scale, m; l_T, Taylor scale, m; M, Mach number; p, pressure, Pa; P, term of turbulence production, m^2/sec^3; Pr, Prandtl number; q, heat flow, W/m^2; **Q**, vector of conservative variables; Re, Reynolds number; S, tensor of deformation rates; St, Strouhal number; t, time, sec; T, temperature, K; u, longitudinal velocity, m/sec; v_x, v_y, v_z, velocity components in the Cartesian coordinate system, m/sec; v_x, v_r, v_θ, velocity components in the cylindrical coordinate system, m/sec; **v**, velocity vector, m/sec; V, volume, m^3; x, y, z, Cartesian coordinates, m; x, r, θ, cylindrical coordinates, m; X, argument of the Heaviside function; α, amplitude of disturbances, m; γ, relation between the specific heat capacities; δ, momentum thickness of boundary layer, m; δ_{ij}, Kronecker symbol; Δ, thickness of the filter, m; ε, rate of turbulent-energy dissipation, m^2/sec^3; λ, heat conductivity, W/(m·K); μ, dynamic viscosity, kg/(m·sec); ρ, density, kg/m^3; σ_k, σ_ε, constants of the model of turbulence; τ, shear stress, N/m; φ, random number; **Ω**, velocity vortex. Subscripts: a, nozzle-exit section; c, axis; e, effective; i, j, tensor indices; min, minimum; max, maximum; s, subgrid; t, turbulent.

REFERENCES

1. G. N. Abramovich, T. A. Girshovich, S. Yu. Krasheninnikov, A. N. Sekundov, and I. P. Smirnova (G. N. Abramovich Ed.), *The Theory of Turbulent Jets* [in Russian], Nauka, Moscow (1984).
2. A. S. Ginevskii, *The Theory of Turbulent Jets and Wakes* [in Russian], Mashinostroenie, Moscow (1969).
3. I. Wygnanski and H. Fiedler, Some measurements in the self preserving jet, *J. Fluid Mech.*, **38**, 577–621 (1969).
4. G. F. Gorshkov, V. S. Komarov, and V. S. Terpigor'ev, Some results of measurements of the average and longitudinal velocity fluctuations in the initial region of an axisymmetric subsonic jet, in: *Hydrodynamics and Elasticity Theory* [in Russian], Izd. DGU, Dnepropetrovsk (1973), pp. 46–52.
5. L. Boguslawski and C. O. Popel, Flow structure of free round turbulent jet in the initial region, *J. Fluid Mech.*, **90**, 531–539 (1979).
6. R. A. Antonia, B. R. Satyaprakash, and A. K. Hussain, Measurements of dissipation rate and some other characteristics of turbulent plane and circular jets, *Phys. Fluids*, **23**, No. 4, 695–700 (1980).
7. N. R. Panchapakesan and J. L. Lumley, Turbulence measurements in axisymmetric jets of air and helium, *J. Fluid Mech.*, **246**, 197–223 (1993).

8. J. Hussein, P. Capp, and K. George, Velocity measurements in a high-Reynolds number, momentum conserving, axisymmetric turbulent jet, *J. Fluid Mech.*, **258**, 31–75 (1994).
9. Y. Antoine, F. Lemoine, and M. Lebouche, Turbulent transport of a passive scalar in a round jet discharging into a co-flowing stream, *Eur. J. Mech. B*, *Fluids*, **20**, 275–301 (2001).
10. B. P. Beloglazov and A. S. Ginevskii, Influence of the initial turbulence and the initial turbulence scale on the characteristics of cocurrent jets, *Prom. Aérodin.*, Issue 1, 195–212 (1986).
11. A. E. Usachov, Numerical investigation of axisymmetric jets with the use of differential model of turbulence, *Prom. Aérodin.*, Issue 6, 124–132 (1991).
12. B. E. Launder, G. J. Reece, and W. Rodi, Progress in the development of a Reynolds stress turbulence closure, *J. Fluid Mech.*, **68**, 537–566 (1975).
13. S. M. Belotserkovskii and A. S. Ginevskii, *Simulation of Turbulent Jets and Wakes on the Basis of the Method of Discrete Vortices* [in Russian], Fizmatlit, Moscow (1995).
14. J. B. Freund, P. Moin, and S. K. Lele, Compressibility effects in a turbulent annular mixing layer, *Technical Report*, Stanford University, Department of Mechanical Engineering, Flow Physics and Computation Division, No. TF-72 (1997).
15. H. Yan and M. Su, Application and comparison of two gas models in large eddy simulation of free turbulent jet flow, *Commun. Nonlinear Sci. Numer. Simul.*, **4**, No. 1, 12–19 (1999).
16. D. A. Lyubimov, The possibilities of using direct methods for numerical simulation of turbulent jets, *Aéromekh. Gaz. Din.*, No. 3, 14–20 (2003).
17. M. Salinas-Vazquez, W. Vicente, A. Espinosa, and E. Barrios, Large eddy simulation of an ammonia jet, *Am. J. Appl. Sci.*, **2**, No. 8, 1270–1273 (2005).
18. B. B. Ilyushin and D. V. Krasinskii, Simulation of the dynamics of a turbulent round jet by the method of large vortices, *Teplofiz. Aéromekh.*, **13**, No. 1, 49–61 (2006).
19. B. J. Boersma and S. K. Lele, Large eddy simulation of compressible turbulent jets, *Center for Turbulence Research. Annual Research Brief*, 365–377 (1999).
20. A. Hilgers, Control and optimization of turbulent jet mixing, *Center for Turbulence Research. Annual Research Brief*, 45–54 (2000).
21. M. Meinke, W. Schroder, E. Krause, and Th. Rister, A comparison of second- and sixth-order methods for large-eddy simulations, *Computers Fluids*, **31**, No. 4–7, 695–718 (2002).
22. M. L. Shur, P. R. Spalart, M. Kh. Strelets, and A. K. Travin, Towards the prediction of noise from jet engines, *Int. J. Heat Fluid Flow*, **24**, No. 4, 551–561 (2003).
23. P. G. Tucker, Novel MILES computations for jet flows and noise, *Int. J. Heat Fluid Flow*, **25**, No. 4, 625–635 (2004).
24. C. Bogey and C. Bailly, Large eddy simulations of round free jets using explicit filtering with/without dynamic Smagorinsky model, *Int. J. Heat Fluid Flow*, **27**, No. 4, 603–610 (2006).
25. B. E. Launder, A. Morse, W. Rodi, and D. B. Spalding, Prediction of free shear flows. A comparison of the performance of six turbulence models, *NASA Report*, No. SP-321, 361–422 (1973).
26. A. Yakhot, S. A. Orszag, V. Yakhot, and M. Israeli, Renormalization group formulation of large-eddy simulation, *J. Sci. Comput.*, **1**, 1–51 (1986).
27. M. P. Martin, U. Piomelli, and G. V. Candler, Subgrid-scale models for compressible large-eddy simulations, *Theor. Comput. Fluid Dynamics*, **13**, 361–376 (2000).
28. S. F. Berch, A. B. Lebedev, D. A. Lyubimov, and A. N. Sekundov, Simulation of turbulent three-dimensional jet and boundary-layer flows, *Izv. Ross. Akad. Nauk*, *Mekh. Zhidk. Gaza*, No. 5, 48–63 (2001).
29. K. N. Volkov, Use of the control-volume method for solving problems of liquid and gas mechanics on unstructured grids, *Vychisl. Metody Programmir.*, **6**, No. 1, 43–60 (2005).